

# Imaging of Merkel Cell Carcinoma: What Imaging Experts Should Know

Gensuke Akaike, MD<sup>1</sup>  
 Tomoko Akaike, MD<sup>1</sup>  
 Shaimaa A. Fadl, MBChB  
 Kristina Lachance, MS  
 Paul Nghiem, MD, PhD  
 Fatemeh Behnia, MD

**Abbreviations:** FDG = fluorodeoxyglucose, MCC = Merkel cell carcinoma, MCPyV = Merkel cell polyomavirus, NCCN = National Comprehensive Cancer Network, NET = neuroendocrine tumor, SLNB = sentinel lymph node biopsy, SSTR = somatostatin receptor

**RadioGraphics** 2019; 39:2069–2084

<https://doi.org/10.1148/rg.2019190102>

**Content Codes:**   

From the Division of Nuclear Medicine, Department of Radiology (G.A., F.B.), and Division of Dermatology, Department of Medicine (T.A., K.L., P.N.), University of Washington, 1959 NE Pacific St, Box 356113, Seattle, WA 98195-6113; and Department of Radiology, Virginia Commonwealth University Health System, Richmond, Va (S.A.F.). Recipient of a Certificate of Merit award for an education exhibit at the 2018 RSNA Annual Meeting. Received April 8, 2019; revision requested May 16 and received June 9; accepted June 26. For this journal-based SA-CME activity, the authors G.A. and P.N. have provided disclosures (see end of article); all other authors, the editor, and the reviewers have disclosed no relevant relationships. **Address correspondence to G.A.** (e-mail: [akagnsk@uw.edu](mailto:akagnsk@uw.edu)).

<sup>1</sup>G.A. and T.A. contributed equally to this work.

©RSNA, 2019

## SA-CME LEARNING OBJECTIVES

After completing this journal-based SA-CME activity, participants will be able to:

- Describe the epidemiology, pathophysiology, unique clinical manifestation, and current treatment strategy of MCC.
- Discuss the important role of imaging in management of MCC.
- List the unique imaging characteristics of MCC as an aggressive cutaneous NET with somatostatin expression.

See [rsna.org/learning-center-rg](http://rsna.org/learning-center-rg).

Merkel cell carcinoma (MCC) is a rare and aggressive cutaneous neuroendocrine tumor with a higher mortality rate than melanoma. Approximately 40% of MCC patients have nodal or distant metastasis at initial presentation, and one-third of patients will develop distant metastatic disease over their clinical course. Although MCC is rare, its incidence has been steadily increasing. Furthermore, the immunogenicity of MCC and its diagnostic and therapeutic application have made MCC one of the most rapidly developing topics in dermatology and oncology. Owing to the aggressive and complex nature of MCC, a multidisciplinary approach is necessary for management of this tumor, including dermatologists, surgeons, radiation oncologists, medical oncologists, pathologists, radiologists, and nuclear medicine physicians. Imaging plays a crucial role in diagnosis, planning for surgery or radiation therapy, and assessment of treatment response and surveillance. However, MCC is still not well recognized among radiologists and nuclear medicine physicians, likely owing to its rarity. The purpose of this review is to raise awareness of MCC among imaging experts by describing the epidemiology, pathophysiology, and clinical features of MCC and current clinical management with a focus on the role of imaging. The authors highlight imaging findings characteristic of MCC, as well as the clinical significance of CT, MRI, sentinel lymph node mapping, fluorine 18 fluorodeoxyglucose PET/CT, and other nuclear medicine studies such as bone scintigraphy and somatostatin receptor scintigraphy.

©RSNA, 2019 • [radiographics.rsna.org](http://radiographics.rsna.org)

## Introduction

Merkel cell carcinoma (MCC) is a rare and highly aggressive cutaneous malignant neuroendocrine tumor (NET). MCC was named on the basis of its ultrastructural and immunophenotypic resemblance to sensory Merkel cells in the base of the epidermis to the dermis, which serve as touch receptors (Fig 1) (1,2). However, the cell of origin for MCC is not yet fully understood. MCCs are most frequently found in the dermis but can manifest clinically in any layer of the skin, from intraepidermal to subcutaneous tissues (3).

Although MCC is a rare skin cancer, its incidence has been increasing strikingly. In 2013, the incidence of MCC in the United States was reported to be approximately 2500 cases per year. This is expected to rise to 2800 cases in 2020 and 3200 cases in 2025 owing to the aging baby boomer population (4). The increasing incidence is noticeable even compared with that of other neoplasms. During 2000–2013, the total number of MCC cases was reported to have increased by 95%, while all solid tumor cases increased by 15% and melanoma by 57% (4).

## TEACHING POINTS

- A baseline MCPyV oncoprotein antibody test is useful for all newly diagnosed MCC patients to assist in following the patient during his or her clinical course.
- Careful assessment of the surrounding cutaneous region is needed, as MCC has a tendency to “jump” discontinuously to adjacent normal-appearing skin, and in-transit and satellite cutaneous metastases can occur.
- Patients with a positive SLNB result have a higher risk of in-transit recurrence and may benefit from adjuvant radiation therapy with inclusion of the in-transit field in amenable cases.
- MCC has a high propensity for nodal metastasis, with 27%–31% of patients presenting with clinical nodal disease. In addition, another 16%–38% have occult nodal metastasis demonstrated at SLNB.
- MCC is a unique cutaneous NET and exhibits SSTR on the tumor cell surface. Like other NETs, MCC has a higher affinity for SSTR types 2A and 5. Owing to these characteristics, a certain radioisotope can be linked to a peptide that binds to SSTR and used for gamma camera imaging or PET or peptide receptor radiation therapy.

The mortality rate is reported to be as high as 33%, much higher than that of malignant melanoma (5–7). Approximately 40% of MCC patients have nodal or distant metastasis at initial presentation, and one-third will develop distant metastatic disease over their clinical course (4,8–10). Therefore, imaging plays a pivotal role in initial staging, treatment planning, and early detection of recurrence and metastases. However, MCC is still not well recognized among radiologists, likely owing to its rarity. In this article, we review the fundamental features of MCC, up-to-date diagnostic and therapeutic approaches, and the role of imaging.

## Clinical Features

MCC typically develops rapidly and manifests as a firm, nontender, dome-shaped red, purple, violet, or skin-colored nodule (Fig 2). It has a predilection for sun-exposed areas but can occur anywhere on the body. In a large analysis of 9387 MCC cases, the most frequent site of the primary tumor was the head and neck (43%), upper limbs and shoulder (24%), lower limbs and hip (15%), trunk (11%) and others (9%) (9). Risk factors for MCC include sun exposure, advanced age, male gender, fair skin, and chronic immune suppression (11–13). Among immunosuppressed patients, the risk of developing MCC is approximately eight times greater in those with human immunodeficiency virus (HIV) infection, 25 times greater in those with organ transplants, and 40 times greater in those with chronic lymphocytic leukemia (13–15).

These significant features of MCC have been summarized in the acronym AEIOU. Indeed,

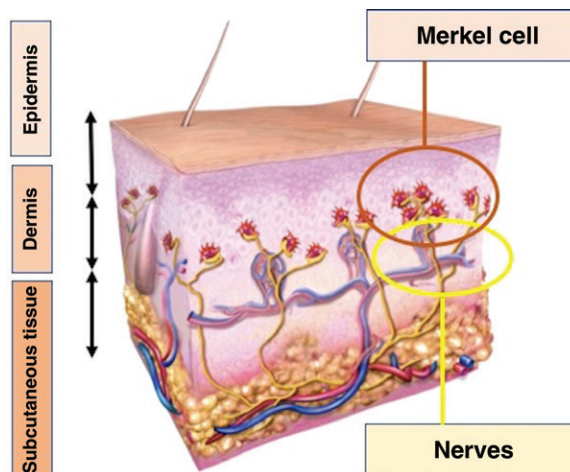


**Figure 1.** Merkel cells (red oval) are located at the base of the epidermis close to the epidermal-dermal interface. They function as touch receptors and are connected to the nerves (yellow oval) responsible for sending touch sensation signals. (Reprinted, with permission, from <https://www.merkelcell.org>.)

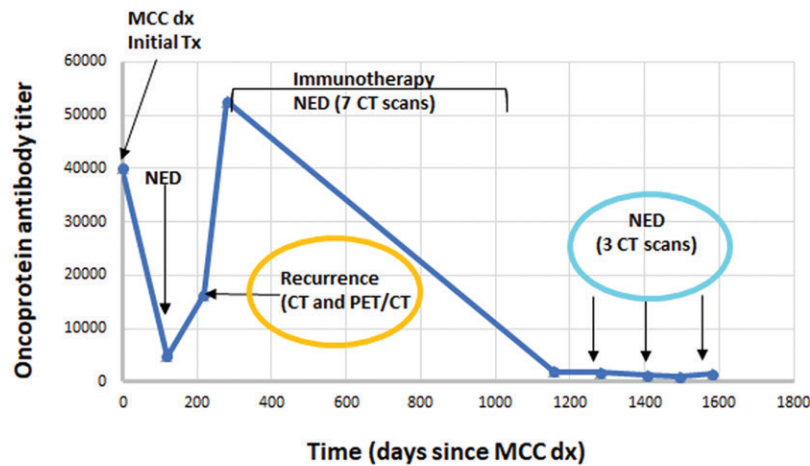


**Figure 2.** Photograph shows a large, nontender, firm MCC tumor (arrows) arising on a sun-exposed area of the left arm. (Reprinted, with permission, from <https://www.merkelcell.org>.)

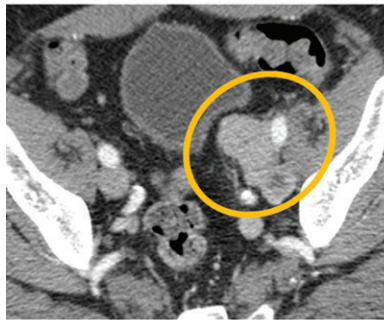
89% of MCC patients present with three or more of the AEIOU characteristics: *a*symptomatic or lack of tenderness, *e*xpanding rapidly, *i*mmune suppression, *o*lder than 50 years, and *u*ltraviolet radiation–exposed site on a person with fair skin (13). However, the dermatologic manifestations of MCC are nonspecific and could be initially interpreted as a benign cutaneous lesion such as a cyst, folliculitis, or a lipoma. A review of 195 MCC patients reported that the majority of MCC lesions (56%) were presumed to be benign at biopsy (13). Therefore, MCC-specific management is usually initiated after a surprising pathology result has been received by the clinician.

## Causative Factors

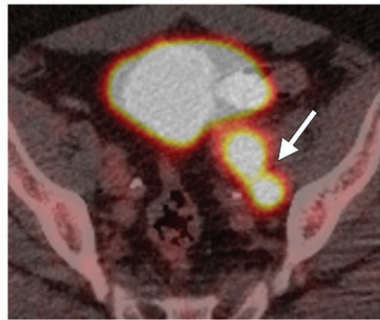
The Merkel cell polyomavirus (MCPyV) was discovered in 2008 (12). Although MCPyV infection itself is common and does not directly cause



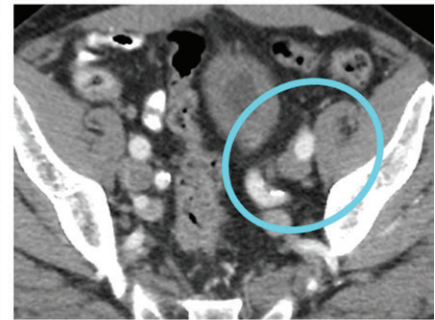
a.



b.



c.



d.

**Figure 3.** MCPyV oncoprotein antibody titer trend in a 71-year-old man with stage pIIA MCC of the left buttock. (a) The baseline serology titer was 40 000. After initial treatment (*Tx*) (wide local excision, sentinel lymph node biopsy [SLNB] with negative results, adjuvant radiation therapy to the primary site), the titer drastically decreased. Seven months after initial diagnosis (*dx*), the serology titer rapidly increased. *NED* = no evidence of disease. (b) Contrast-enhanced CT image shows an enhancing mass in the left iliac region (yellow oval). (c) Fluorodeoxyglucose (FDG) PET/CT image shows that the mass is hypermetabolic (arrow), consistent with metastasis. The patient underwent immunotherapy (pembrolizumab for 2 years) with a complete response. The serology titer subsequently decreased. (d) Follow-up contrast-enhanced CT image shows no evidence of disease (blue oval).

problems, it is causally linked to 80% of MCC cases in the United States, whereas the remaining 20% are caused by extensive ultraviolet radiation mutations (12).

### MCPyV Serology Test

Studies have shown the clinical utility of a serology test detecting antibodies to MCPyV oncoproteins (T antigens). About half of MCC patients produce antibodies to MCPyV oncoproteins at diagnosis (16). A baseline MCPyV oncoprotein antibody test is useful for all newly diagnosed MCC patients to assist in following the patient during his or her clinical course. The clinical practice guidelines of the National Comprehensive Cancer Network (NCCN) recommend considering quantification of MCPyV oncoprotein antibodies as part of the initial workup for patients with MCC (17).

If patients are seropositive at diagnosis, a rising titer may be an early indicator of recurrence (Fig 3). For seropositive patients, this test may be used for surveillance and may reduce

imaging studies, decreasing the cost and radiation exposure of imaging and the toxic effects of contrast material (16). If patients are seronegative at initial diagnosis, their risk of recurrence is 42% higher than that of seropositive patients, and close surveillance with more frequent imaging is needed (16). The antibody test is not used beyond this baseline determination in patients who do not produce antibodies.

### Staging and Prognosis

The American Joint Committee on Cancer (AJCC) TNM staging system, eighth edition, is the most widely used staging system (9). Each stage is divided into a clinical stage and a pathologic stage. Clinical detection of disease may be via inspection, palpation, or imaging. Pathologic detection of nodal or distant metastatic disease may be via sentinel lymph node biopsy (SLNB), lymph adenectomy, or fine-needle or standard biopsy of the suspected metastasis.

Stage I tumors are equal to or smaller than 2 cm in maximum dimension. Stage II tumors have

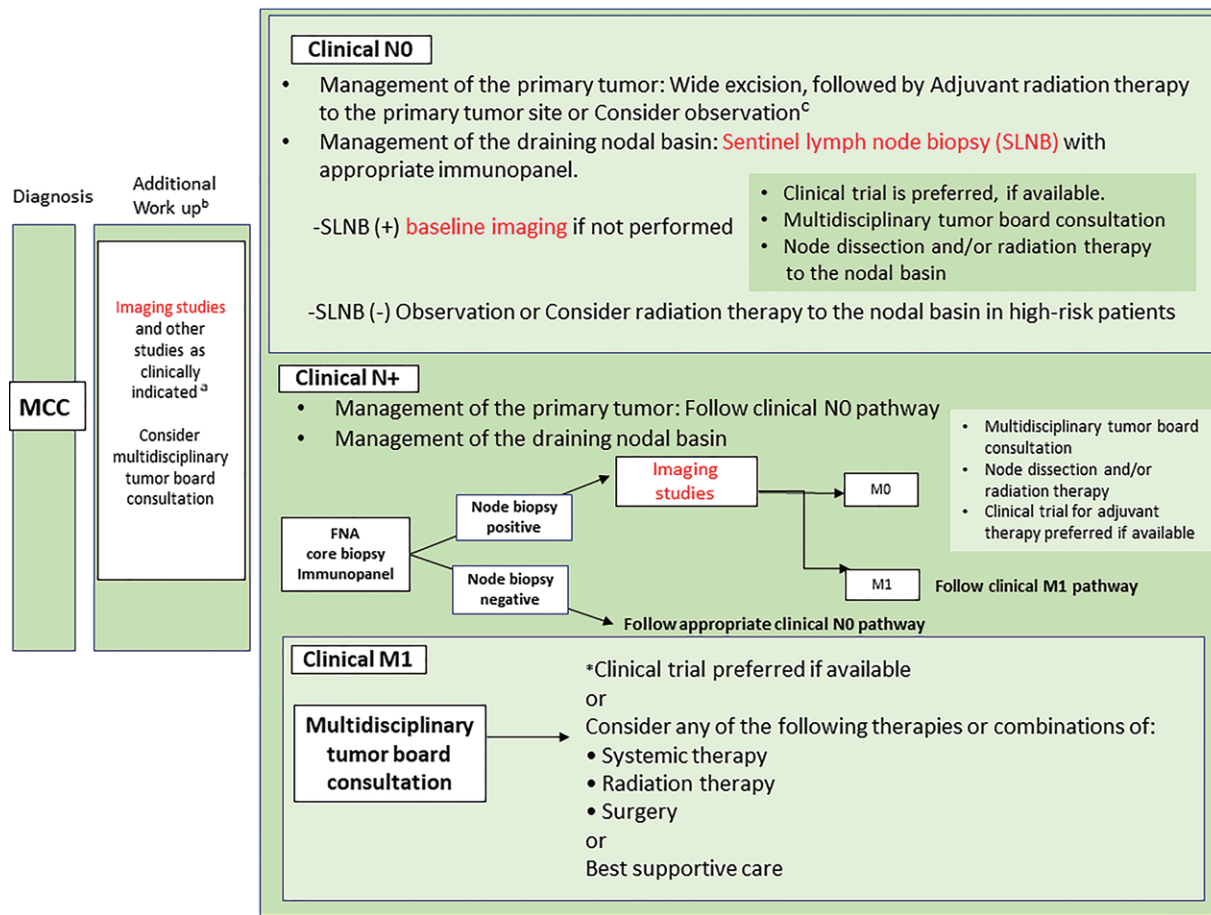


**Figure 4.** Management of MCC. *a*, Imaging is encouraged whenever metastatic or unresectable disease is suspected on the basis of the history and physical examination findings. The most reliable staging tool for identifying subclinical nodal disease is SLNB. *b*, Quantitation of MCPyV oncoprotein antibodies may be considered part of the initial workup. Seronegative patients may have a higher risk of recurrence; in seropositive patients, a rising titer may be an early indicator of recurrence. *c*, Consider observation of the primary site in cases where the primary tumor is small (eg, <1 cm) and widely excised with no other adverse risk factors such as lymphovascular invasion or immunosuppression. FNA = fine-needle aspiration, - = negative, + = positive. (Adapted and reprinted, with permission, from reference 17.)

a maximum dimension of greater than 2 cm or bone, muscle, fascia, or cartilage invasion. Stage III tumors have regional lymph node metastasis. Stage IV tumors have distant metastasis.

Estimated 5-year overall survival is 51%, 35%, and 14% for local, nodal, and distant disease, respectively (9). In the eighth edition AJCC staging system, patients with stage pIII disease with no identifiable primary or an unknown primary are included in the stage pIIIA subgroup because they have a significantly better prognosis than patients with nodal disease and a known primary (stage pIIIB) (9). This may be because improved antitumor immunity eliminated the primary tumor and also targets residual disease (18).

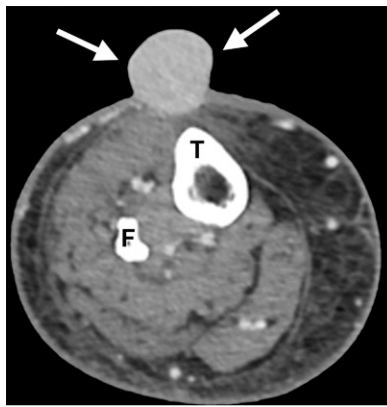
### Role of Imaging

MCC is a unique skin cancer that has many interesting imaging features. Radiology and nuclear medicine play an essential role in its management. Figure 4 is a flowchart for management of MCC from the NCCN clinical practice guidelines (17).

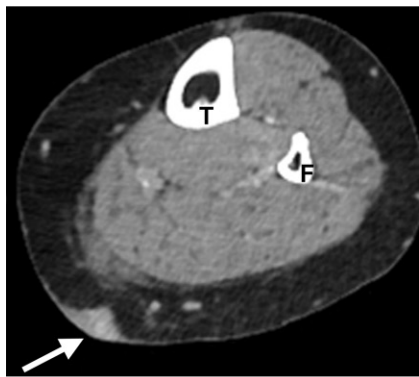
### Imaging of Primary or Regional MCC

The role of imaging in MCC management is primarily to detect regional nodal or distant metastases, as many patients are referred for imaging for staging. The primary lesion may or may not have been resected at the time of imaging. In locally advanced disease or distant metastatic disease, imaging plays an important role in determining the location of the lesion and identifying local-regional invasion to surrounding organs to guide surgical or radiation therapy planning. This is especially essential in head and neck disease, owing to its anatomic complexity. The primary MCC lesion may be detected incidentally at routine imaging for other reasons (19). Careful assessment of the surrounding cutaneous region is needed, as MCC has a tendency to “jump” discontinuously to adjacent normal-appearing skin, and in-transit and satellite cutaneous metastases can occur (20).

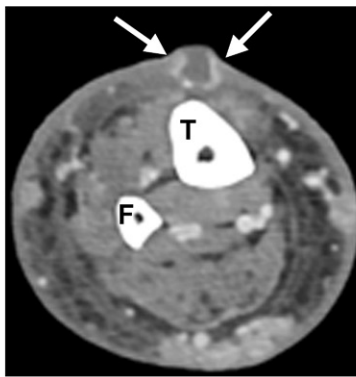
Although MCC has nonspecific imaging features, there are evocative findings associated with



a.



b.



c.



d.

**Figure 5.** Imaging findings of primary MCC. In **a–c**, *F* = fibula and *T* = tibia. **(a)** MCC in an 81-year-old woman. Axial contrast-enhanced CT image of the right leg shows an exophytic soft-tissue nodule (arrows) from the skin along the anterior aspect of the leg. **(b)** MCC in a 54-year-old woman. Axial contrast-enhanced CT image of the left leg shows focal skin thickening (arrow) along the posterior medial aspect of the leg. **(c)** MCC in an 80-year-old woman. Axial contrast-enhanced CT image of the right leg shows a necrotic cutaneous nodule along the anterior aspect of the leg (arrows). **(d)** MCC in a 66-year-old woman. Axial contrast-enhanced CT image of the chest shows an enhancing subcutaneous soft-tissue nodule (arrow).

it that are helpful. Common features of a primary MCC include a cutaneous or subcutaneous nodule (sessile or fungating cutaneous nodule or mass) and focal or diffuse skin thickening (Fig 5). It can manifest as a perifascial muscular or intramuscular mass (Fig 6). Necrosis is common, whereas calcifications are not.

At CT, cutaneous fat stranding near the primary MCC may suggest the presence of engorgement and edema from lymphatic invasion (21). Often, there is large lymph node enlargement with fine compressed or retained fatty tissue (22). US can be used, especially for MCC in the head and neck (23). US evaluation of primary MCC usually demonstrates hypoechoic nodules arising from the dermis and extending into the subcutaneous fat, with variable degrees of posterior acoustic transmission (21). US enables real-time imaging with possible simultaneous fine-needle or core-needle biopsy and provides a concise workup at lower cost.

At MRI, MCC is hypo- to isointense on T1-weighted images and iso- to hyperintense on T2-weighted images or fat-saturated T2-weighted images (24,25). On gadolinium-enhanced images, the lesion usually has diffuse or heterogeneous enhancement. Large lesions can have inhomogeneous signal intensity on both T1- and T2-weighted images. Focal central increased sig-

nal intensity within large lesions on T2-weighted images has been described as being associated with central necrosis and hemorrhage (24).

At histologic analysis, the skin, subcutaneous mass, and reticular stranding are found to be involved by lymphangitic carcinomatosis and soft-tissue lymphatic metastases. MCC is a highly metabolic tumor and demonstrates intense fluorine 18 ( $^{18}\text{F}$ ) fluorodeoxyglucose (FDG) uptake at PET. The mean maximum SUV (standardized uptake value) at  $^{18}\text{F}$ -FDG PET for a primary MCC is reported to be 4–6.5 (26,27). Also, MCC often expresses increased somatostatin receptor (SSTR) on its surface and therefore shows increased radiotracer uptake at somatostatin-seeking scintigraphy and PET/CT (discussed later).

### Sentinel Lymph Node Biopsy

SLNB is the most reliable tool for investigating subclinical nodal metastases. The NCCN guidelines recommend SLNB for all clinically node-negative patients who are fit for surgery because it is an important staging tool and in combination with subsequent treatment affects regional control for those with positive sentinel lymph nodes (28). Patients with a positive SLNB result have a higher risk of in-transit recurrence and may benefit from adjuvant radiation therapy with inclusion of the in-transit field in amenable cases

(29). In patients with stage I and II MCC, SLNB is more sensitive than  $^{18}\text{F}$ -FDG PET/CT (30). SLNB should be performed before wide local excision or Mohs micrographic surgery because surgical excision before SLNB may alter the lymphatic drainage patterns.

At our institution, technetium 99m ( $^{99\text{m}}\text{Tc}$ ) sulfur colloid (1 mCi [ $37 \times 10^6$  Bq], 0.2  $\mu\text{m}$  filtered) is used for lymphoscintigraphic sentinel lymph node mapping (Fig 7). The dose is injected intradermally at four locations around the primary tumor or tumor biopsy site. Multiple static images of the expected lymph nodal basin are obtained to localize the sentinel lymph node. A handheld gamma probe is used to confirm the node.

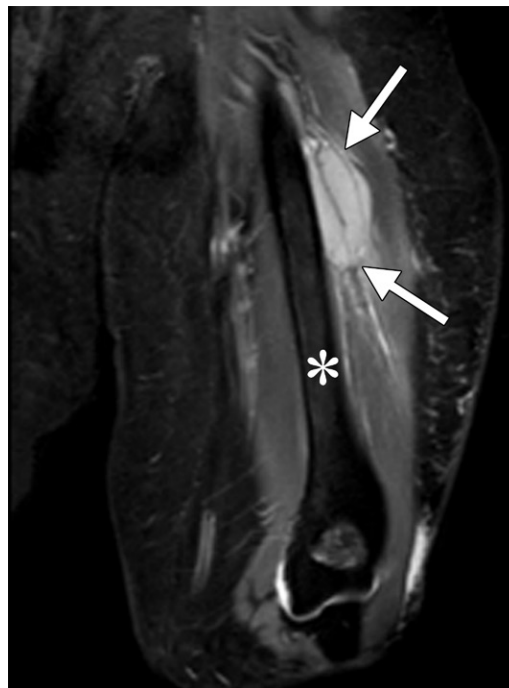
For anatomically complex areas or when planar images are difficult to interpret, SPECT/CT can be performed to localize the sentinel lymph node. In addition, the higher sensitivity and spatial and contrast resolution of SPECT allow visualization of foci undetected on planar images. At our institution, SPECT/CT is routinely performed for MCC of the head and neck owing to its anatomic complexity. The sentinel lymph node is further localized with blue dye in the operating room. The combination of the two mapping methods is an accurate approach and widely performed.

### Detecting Nodal or Distant Metastasis

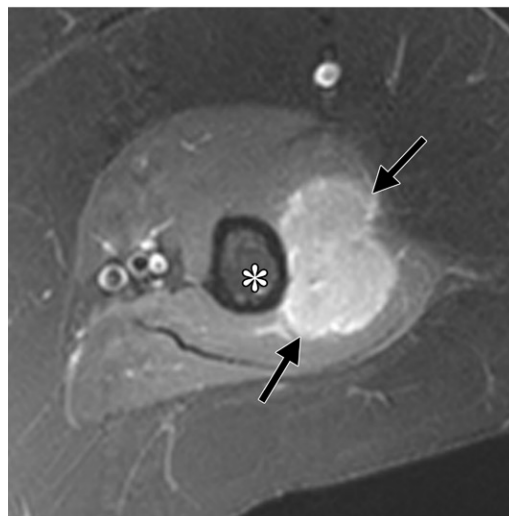
MCC has a high propensity for nodal metastasis, with 27%–31% of patients presenting with clinical nodal disease. In addition, another 16%–38% have occult nodal metastasis demonstrated at SLNB (29). On the basis of various large patient databases, the most frequent distant metastasis site is a nonregional lymph node, occurring in 33%–85% of cases, followed by the skin or subcutaneous tissue, bones, liver, and lung or pleura (26,31–33). Less frequent sites include the pancreas (Fig 8), muscle (Figs 6, 9), central nervous system (Fig 10), adrenal glands, heart (Fig 11), gastrointestinal tract (Fig 12), retroperitoneum, urinary bladder, and breast.

There is no imaging feature specific for MCC metastasis with any modality, and US, CT, MRI, or PET/CT can be used as indicated. Imaging findings of MCC metastasis have been described only in several case reports, case series, or review articles. MCC metastasis can manifest as lymphadenopathy, a cutaneous or subcutaneous soft-tissue nodule, a pulmonary nodule or masses, or related chest wall invasion.

A solid visceral metastasis in the abdomen tends to be hypervascular with peripheral rim enhancement at contrast-enhanced CT or MRI and hypoattenuating or hypointense in the portal venous phase (19,34,35) (Fig 8). Metastasis to



a.



b.

**Figure 6.** Regional metastasis in a 70-year-old woman with MCC of the distal left arm who underwent resection and radiation therapy and presented with new radial nerve palsy. (a) Coronal fat-saturated T2-weighted MR image of the left arm shows an oval hyperintense mass (arrows) involving the triceps and brachialis muscles adjacent to the humerus (\*) and proximal to the resection site. (b) Axial contrast-enhanced T1-weighted MR image shows the enhancing mass (arrows) abutting the humerus (\*) and involving the location of the radial nerve.

hollow organs such as the stomach or bowel can manifest as wall thickening or a wall mass, ulceration (19), or bowel thickening with aneurysmal dilatation (Fig 12). A bone metastasis can be osteolytic or osteoblastic at radiography or CT (36). MRI can be used for detection of bone marrow involvement and extraosseous extension (37).

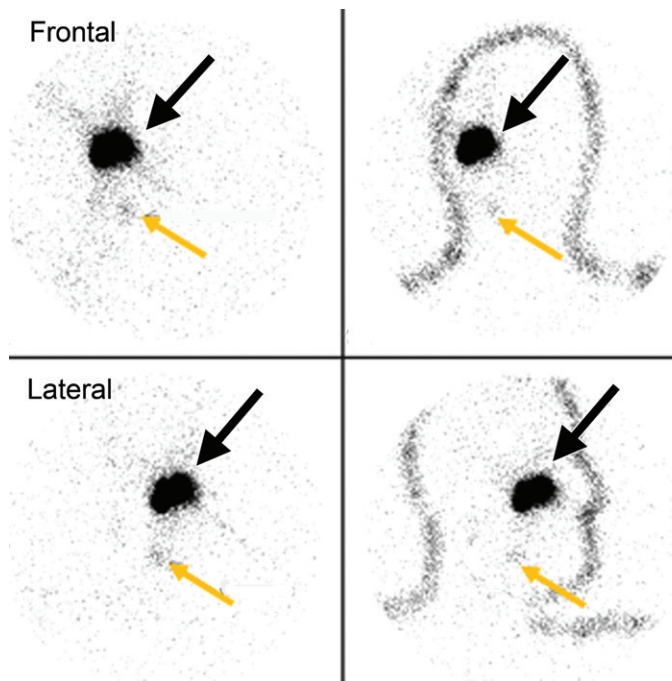


**Figure 7.** MCC in a 72-year-old woman referred for sentinel lymph node mapping. (a) Anterior and lateral images of the head and neck from <sup>99m</sup>Tc sulfur colloid scintigraphy show a large focus of intense radiotracer uptake (black arrows) within the right cheek, which corresponds to the intradermal injection site around the primary tumor. A fainter smaller focus of radiotracer uptake (yellow arrows) below the injection site suggests the sentinel lymph node. (b) Axial SPECT/CT image shows intense radiotracer uptake at the injection site along the right cheek (arrow). (c) Axial SPECT/CT image shows a focus of increased uptake in the sentinel lymph node adjacent to the right parotid gland (arrow). (d) Axial SPECT/CT image of the neck below the level of the parotid gland shows an additional focus of increased radiotracer uptake in a smaller sentinel lymph node in the submandibular region (arrowhead).

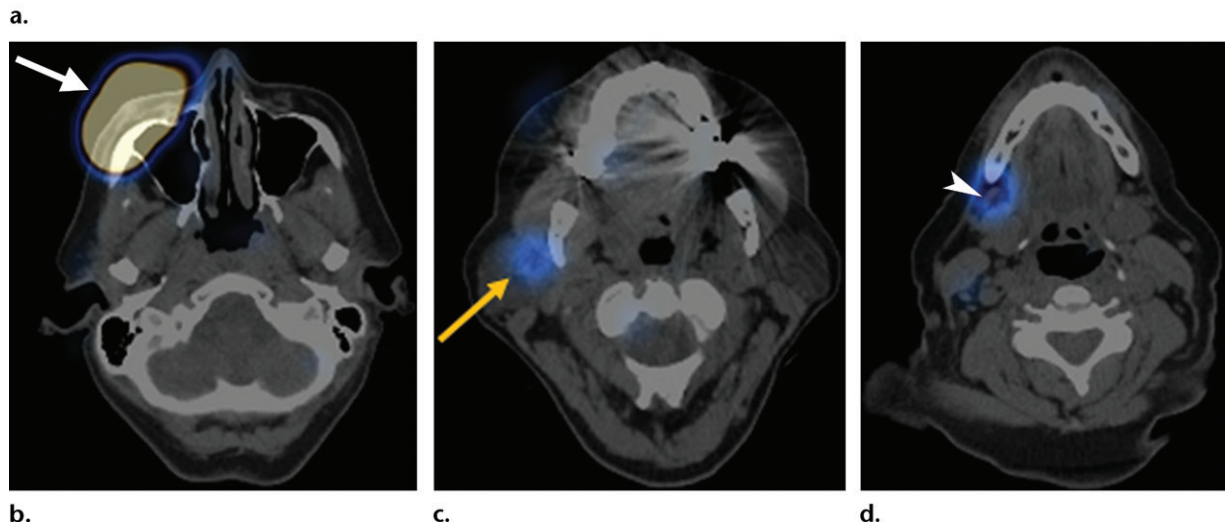


**Figure 8.** Pancreatic metastasis in a 30-year-old man with MCC of the right lower extremity who was referred for staging. Axial contrast-enhanced CT image shows a hypoattenuating exophytic mass (arrows) arising from the pancreas (P). No dilatation of the main pancreatic duct is noted.

Cardiac metastasis is rare. Owing to its invasiveness, it is difficult to achieve pathologic confirmation with biopsy. Thus, imaging is important to establish a diagnosis of this rare manifestation (Fig 11).

<sup>18</sup>F-FDG PET is increasingly used for detection of distant metastasis. MCC is a hypermetabolic tumor with a reported  $SUV_{max}$  (maximum standardized uptake value) for distant metastasis of 7.2–11.5 (26,27). Many studies have indicated favorable performance of <sup>18</sup>F-FDG PET/CT (discussed later). However, <sup>18</sup>F-FDG PET has

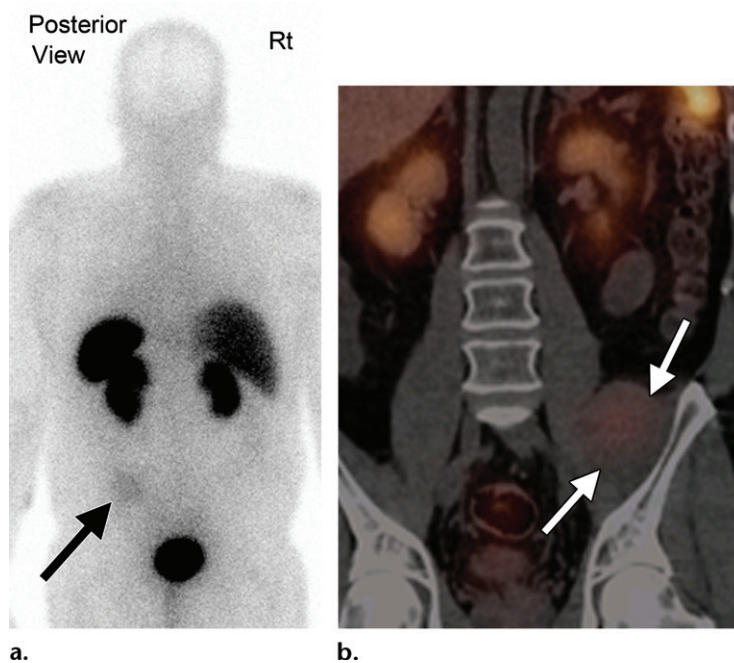


**Figure 9.** Intramuscular metastasis in a 55-year-old man with MCC of the lower extremity. (a) Whole-body posterior image from indium 111 ( $^{111}\text{In}$ )-pentetretotide scintigraphy shows faint increased radiotracer uptake along the left side of the pelvis (arrow). *Rt* = right. (b) Coronal SPECT/CT image shows increased radiotracer uptake in a left iliacus muscle metastasis (arrows).

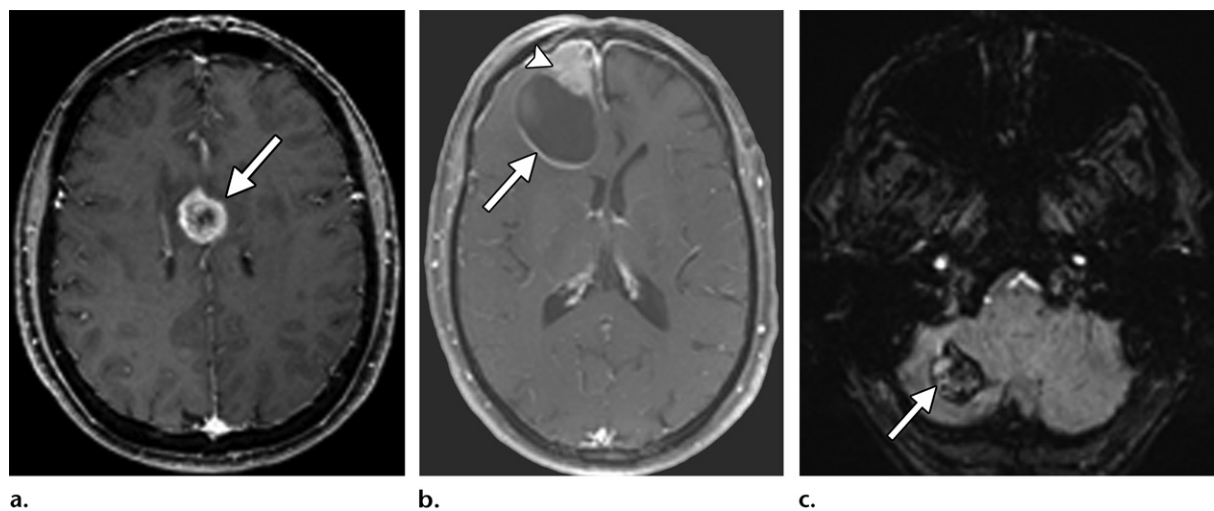


**Figure 10.** Central nervous system metastases in four patients. (a) Brain metastasis in a 67-year-old woman with MCC of the right mandible that was originally staged IIB. Axial contrast-enhanced MR image shows an enhancing lesion (arrow) in the corpus callosum. (b) Complex cystic metastasis in a 65-year-old man with MCC of the forehead. Axial contrast-enhanced MR image shows a predominantly cystic lesion (arrow) in the right frontal lobe with an enhancing solid component (arrowhead). (c) Hemorrhagic metastasis in a 63-year-old man with MCC. Axial susceptibility-weighted image shows a heterogeneous right cerebellar mass (arrow) with areas of low signal intensity indicative of hemorrhage. (d) Epidural metastasis in a 65-year-old man with MCC. Axial contrast-enhanced MR image of the spine shows an enhancing epidural nodule (arrow).

decreased sensitivity for brain metastasis owing to intense physiologic FDG activity in the brain, in which case contrast-enhanced brain MRI should be performed (38).

The reported imaging characteristics of brain metastasis from MCC include an enhancing homogeneous or heterogeneous parenchymal nodule or masses, a cystic mass with or without a mural enhancing nodule, leptomeningeal

metastasis, direct parenchymal invasion from a skull metastasis, or a parenchymal brain metastasis with skull infiltration (Fig 10). Necrosis or hemorrhage can be seen. Lesions may or may

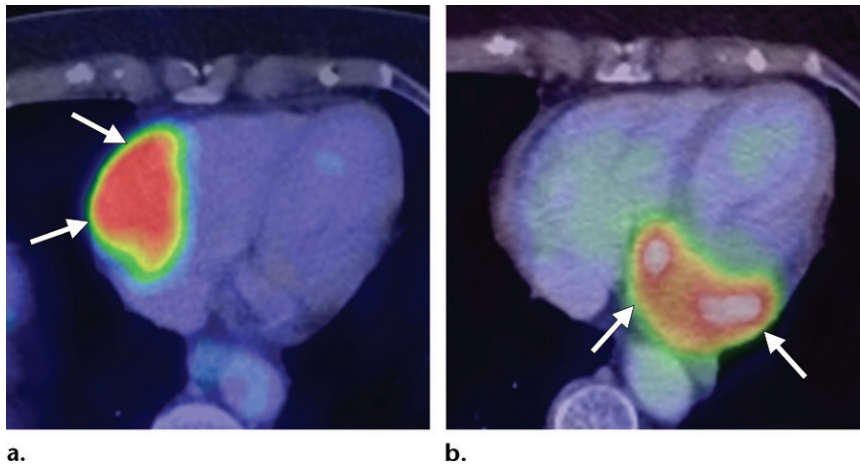


**Figure 11.** Pericardial metastasis in an 80-year-old woman with metastatic MCC. (a) Axial  $^{18}\text{F}$ -FDG PET/CT image shows a hypermetabolic mass (arrows) at the pericardial–right atrial interface. The mass was irradiated and diminished. (b) Axial  $^{18}\text{F}$ -FDG PET/CT image 11 months later shows a pericardial recurrence (arrows) in a different site at the base of the left ventricle.

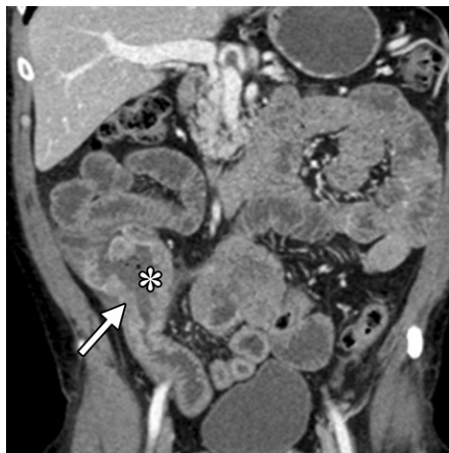


**Figure 12.** Small bowel metastasis in a 58-year-old woman with metastatic MCC. Coronal contrast-enhanced CT image shows thickening of the distal ileal bowel wall (arrow) with aneurysmal dilatation (\*).

not be associated with surrounding vasogenic edema (39–41). Contrast-enhanced MRI is also preferred for diagnosis of spinal metastasis (Fig 10d), and both intradural and extradural metastases to the spine have been reported (40,42–45).

### Treatment

Standard treatment of MCC is generally surgery, radiation therapy, or systemic therapy, depending on staging. According to the NCCN guidelines, wide local excision of the primary lesion is a component of initial management, but surgical margins should be balanced with the morbidity of surgery (17,28). After wide local resection, observation may be reasonable for patients with small primary lesions (eg, <1 cm) that have been widely excised and who present with no risk factors such as lymphovascular invasion or immunosuppression (17).

Adjuvant radiation therapy to the primary site is generally recommended for all other cases,

especially for patients with microscopic or grossly positive margins or other risk factors for recurrence (17). If there is regional nodal involvement (confirmed with biopsy), node dissection and/or radiation therapy to the lymph nodes should be performed. Multidisciplinary tumor board consultation is recommended, and a clinical trial for adjuvant therapy is preferred if available (17).

For MCC patients with distant metastasis, treatment in the context of a clinical trial is preferred if available. Other options to consider include systemic therapy, radiation therapy, and/or surgery (17,28,46). Until 2016, chemotherapy (carboplatin/cisplatin and etoposide or a combination of cyclophosphamide and doxorubicin) was the only systemic treatment option listed in the NCCN guidelines for MCC. However, responses are not durable, with median progression-free survival of about 94 days, and toxic effects are considerable (47).

Recently, immunotherapy such as targeting the PD-1 (programmed cell death 1) pathway was found to activate the immune system to attack tumor cells. PD-1 or PD-L1 (programmed death ligand 1) antibody therapy has demonstrated promising long-term effects (48). On the basis of preliminary data from nonrandomized trials showing promising response rates to PD-1 or PD-L1 blockade, several of these agents (avelumab, nivolumab, and pembrolizumab) are included as recommended systemic therapy options for treatment of disseminated disease in the current NCCN guidelines (17). These agents are the preferred options for patients who select systemic therapy as part of their treatment of disseminated disease (17).

### Follow-up or Assessment of Treatment Response

Currently, there is no consensus regarding the accuracy and utility of imaging modalities for follow-up or assessment of treatment response. For follow-up imaging, the NCCN guidelines

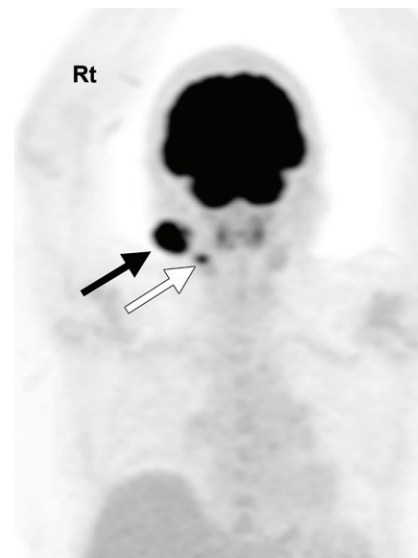
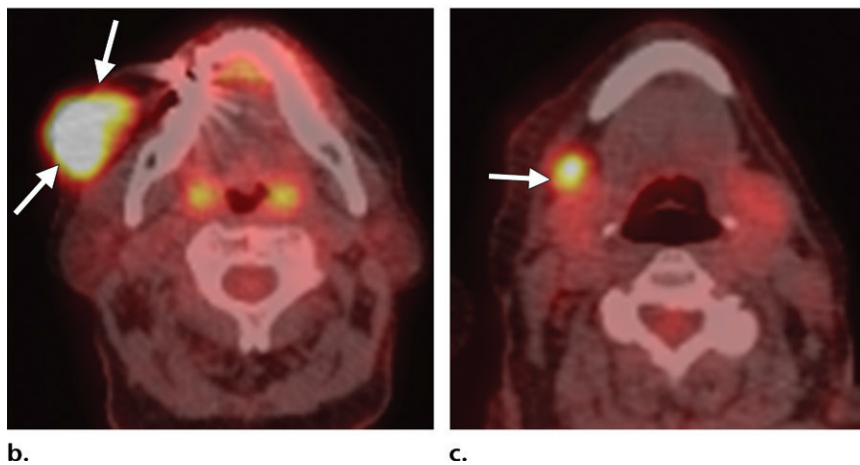


**Figure 13.** MCC of the cheek in a 66-year-old woman who was referred for staging. (a) Whole-body  $^{18}\text{F}$ -FDG PET image shows a hypermetabolic primary mass (black arrow) in the right (Rt) cheek and a metastatic hypermetabolic right submandibular lymph node (white arrow). (b) Axial  $^{18}\text{F}$ -FDG PET/CT image shows the primary mass (arrows) of the right cheek. (c) Axial  $^{18}\text{F}$ -FDG PET/CT image shows the submandibular lymph node (arrow).



recommend imaging studies “as clinically indicated,” such as in the case of emergent adenopathy, unexplained changes in liver function test results, or development of new suspicious symptoms. In addition, routine imaging should be considered for high-risk patients (eg, those stage IIIB or higher or with immunosuppression) (28).

The guideline states that “whole body PET with fused axial imaging (CT or MR) or neck/chest/abdomen/pelvis CT with contrast, with or without brain MRI, may be useful to identify and quantify regional and distant metastases” (17). In clinical practice, interpreting PET/CT or PET/MR images would require reviewing raw PET images and attenuation-corrected CT or MR images in multiple planes in addition to fused axial images. It is important for radiologists to guide the clinical team in terms of which modality is most appropriate in each case.

On the basis of the current guidelines, more MCC patients will receive immunotherapy rather than cytotoxic chemotherapy (17). If imaging is performed in MCC patients receiving immuno-

therapy, these patients may have an unconventional response, and immune-modified Response Evaluation Criteria in Solid Tumors (imRECIST) may better capture the treatment response (49).

For follow-up of MCC patients with bone metastasis receiving radiation therapy or systemic therapy, metabolic change at  $^{18}\text{F}$ -FDG PET better correlates with true disease status than does change at CT. New sclerotic change at CT may be due to treatment response or progressive disease (50). This may be misleading in a sensitive situation like a patient with MCC metastasis receiving radiation therapy or systemic therapy. A decrease in the extent or intensity of FDG activity in the face of increasing sclerosis at CT usually heralds healing (50).

### Role of Specific Nuclear Medicine Studies

#### $^{18}\text{F}$ -FDG PET

$^{18}\text{F}$ -FDG PET/CT is a good modality for staging and is increasingly used, as MCC is usually

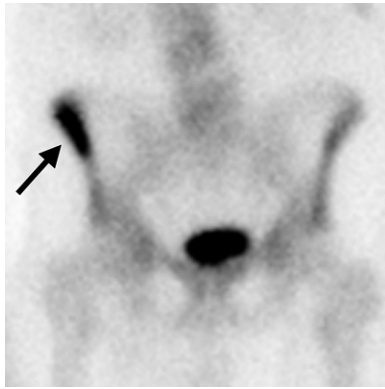


**Figure 14.** Osseous metastasis in a 63-year-old woman with MCC. Image from  $^{99m}\text{Tc}$ -methylene diphosphonate (MDP) bone scintigraphy shows asymmetric increased radiotracer uptake in the right iliac bone (arrow). There was no correlative lesion at CT (not shown), and biopsy demonstrated metastasis.

very FDG avid (Figs 11, 13). According to a large meta-analysis of 10 studies comprising 328 MCC patients who underwent 549  $^{18}\text{F}$ -FDG PET/CT scans,  $^{18}\text{F}$ -FDG PET/CT has sensitivity of 90% and specificity of 98%, allowing pathologic and nonpathologic reference standards (ie, use of clinical or radiologic follow-up as a standard) (51).  $^{18}\text{F}$ -FDG PET/CT is useful for detection of nodal involvement and distant metastasis.  $^{18}\text{F}$ -FDG PET/CT demonstrates more bone metastases than CT (52).

Studies have reported that initial or baseline staging  $^{18}\text{F}$ -FDG PET/CT significantly influenced treatment decisions and management in up to around 40% of patients (26,27,32,53–55). A prospective study of 58 MCC patients (AJCC [American Joint Committee on Cancer] version 7 stages IIA–IIIB) demonstrated that staging  $^{18}\text{F}$ -FDG PET significantly influenced treatment decisions in 27.6% of patients, with disease in 25.9% of patients being upstaged whereas no disease was downstaged (54). In this study, posttreatment PET was not found to be prognostic (54). Another large study of 270 scans in 97 MCC patients reported that initial  $^{18}\text{F}$ -FDG PET/CT led to upstaging in 16% of patients (26).

A retrospective study of 102 consecutive MCC patients demonstrated that initial staging PET had a high clinical impact (the PET results changed the primary treatment modality or intent) in 22% of patients and a medium impact (the treatment modality was unchanged, but the radiation therapy technique or dose was altered) in 15% (53). These authors also reported that the PET stage was significantly associated with overall survival. A smaller retrospective study of 23 MCC patients found that initial PET/CT

led to a change in staging in seven of 18 patients (39%) and a change in treatment in six of 18 patients (33%) (55).

A retrospective study of 62 MCC patients who were treated definitively and underwent posttreatment PET found that restaging  $^{18}\text{F}$ -FDG PET had a high impact (the PET results changed the primary treatment modality or intent) in 24 of 53 cases (45%) and a medium impact (the treatment modality was unchanged, but the radiation therapy technique or dose was altered) in six of 53 cases (11%) (56). Metabolic response was significantly associated with overall survival (56).

More recently, there have been several case reports suggesting the usefulness of  $^{18}\text{F}$ -FDG PET/CT for assessment of immunotherapy response (57,58). Caution is needed for interpretation because  $^{18}\text{F}$ -FDG can also accumulate in inflammation or infection, and careful correlation with CT is necessary.

### Bone Scintigraphy

Bone scintigraphy using bone-seeking radiotracers such as  $^{99m}\text{Tc}$ -methylene diphosphonate (MDP) can be used to detect bone metastasis (Fig 14). It is a relatively concise imaging technique with low cost, and whole-body evaluation is possible. The tracer is a nonspecific radiotracer binding to the hydroxyapatite of the osseous matrix at a site of active bone remodeling (59).

Bone metastasis responding to treatment may cause more bone remodeling or healing and therefore more radiotracer uptake at bone scintigraphy, mimicking progression (flare phenomenon) (60). Multiple meta-analyses have shown that  $^{18}\text{F}$ -FDG PET has higher sensitivity than bone scanning for detecting bone metastasis in other cancers (61–63).

### Somatostatin Receptor-seeking Nuclear Medicine

MCC is a unique cutaneous NET and exhibits SSTR on the tumor cell surface. Like other NETs, MCC has a higher affinity for SSTR types 2A and 5 (64). Owing to these characteristics, a certain radioisotope can be linked to a peptide that binds to SSTR and used for gamma camera imaging or PET or peptide receptor radiation therapy (Fig 15).

Indium 111 ( $^{111}\text{In}$ )-pentetreotide (OctreoScan; Curium, Maryland Heights, Mo) has long been used for scintigraphic imaging of NETs including MCC (Figs 16, 17). It has high affinity for SSTR types 2 and 5, to a lesser extent for type 3, but not for types 1 and 4 (59).

Gallium 68 ( $^{68}\text{Ga}$ ) DOTA (tetraazacyclododecane tetraacetic acid)-Tyr<sup>3</sup>-octreotate

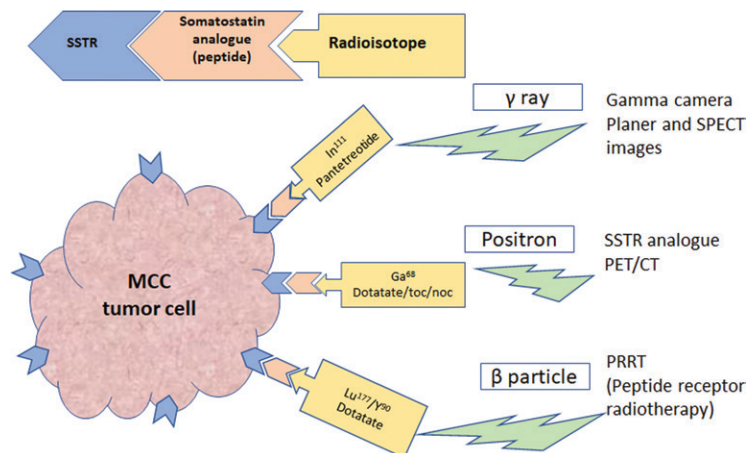
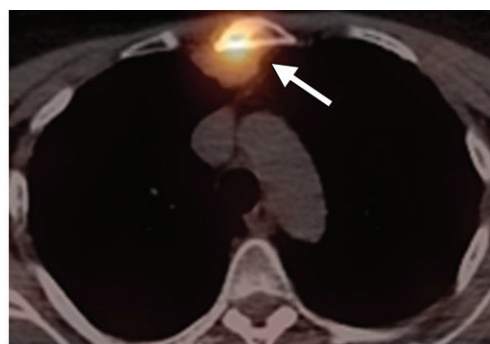
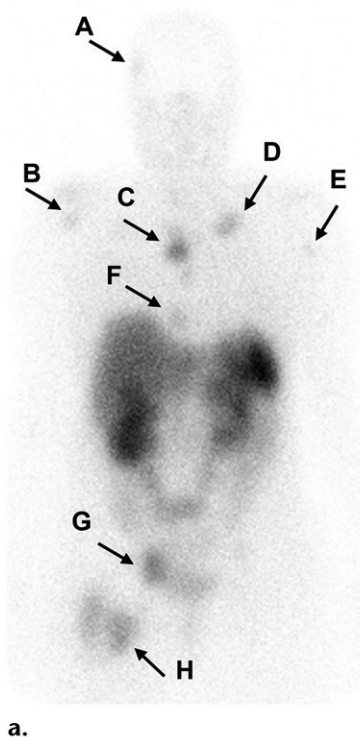
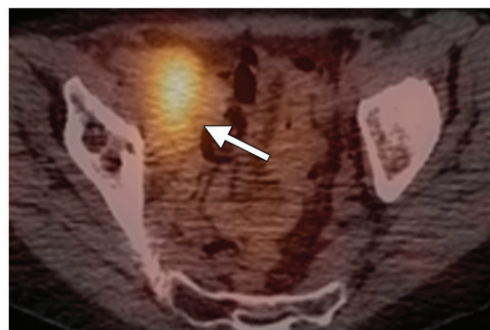


**Figure 15.** Somatostatin analog peptides labeled with different radioisotopes that can be used in diagnostic imaging ( $^{111}\text{In}$ -pentetreotide, gallium 68 [ $^{68}\text{Ga}$ ]-DOTATATE) or peptide receptor radionuclide therapy (PRRT) (lutetium 177 [ $^{177}\text{Lu}$ ], yttrium 90 [ $^{90}\text{Y}$ ]).

**Figure 16.** Widespread metastases in a 69-year-old woman with MCC of the left arm. (a) Whole-body  $^{111}\text{In}$ -pentetreotide image shows several foci of increased radiotracer uptake compatible with metastasis having SSTR expression (arrows), some with higher uptake than the liver. The areas of metastasis include the right side of the calvaria (A), right scapula (B), sternum (C), left subpectoral region (D), left proximal humerus (E), right cardiophrenic angle (F), right external iliac node (G), and soft tissue around the right proximal femur (H). (b–d) Axial SPECT/CT images show the sternal metastasis (arrow in b), the right external iliac node metastasis (arrow in c), and the metastasis in the soft tissue around the right femur (arrow in d).



b.



c.



d.

(DOTATATE),  $^{68}\text{Ga}$  DOTA- $\text{NaI}^3$ -octreotide (DOTANOC), and  $^{68}\text{Ga}$  DOTA-TyI $^3$ -octreotide (DOTATOC) are PET tracers with high affinity for SSTR and can be used for imaging of NETs including MCC (Fig 18). In the United States, the Food and Drug Administration (FDA) recently approved  $^{68}\text{Ga}$ -DOTATATE for imaging of NETs. The advantages of  $^{68}\text{Ga}$ -labeled somatostatin analog PET over  $^{111}\text{In}$ -pentetreotide imaging are higher spatial resolution and sensitivity, shorter scanning time, and the fact that quantification of several parameters such as standardized uptake value (SUV) is possible.

With  $^{68}\text{Ga}$ -labeled somatostatin analog PET, a patient can be scanned 45–60 minutes after radiotracer administration, whereas  $^{111}\text{In}$ -labeled pentetreotide imaging is typically performed 24–

72 hours after radiotracer administration. It is reported that SSTR analog PET has higher sensitivity for bone, soft-tissue, and brain disease than CT but lower sensitivity for liver and lung disease, stressing the importance of combined

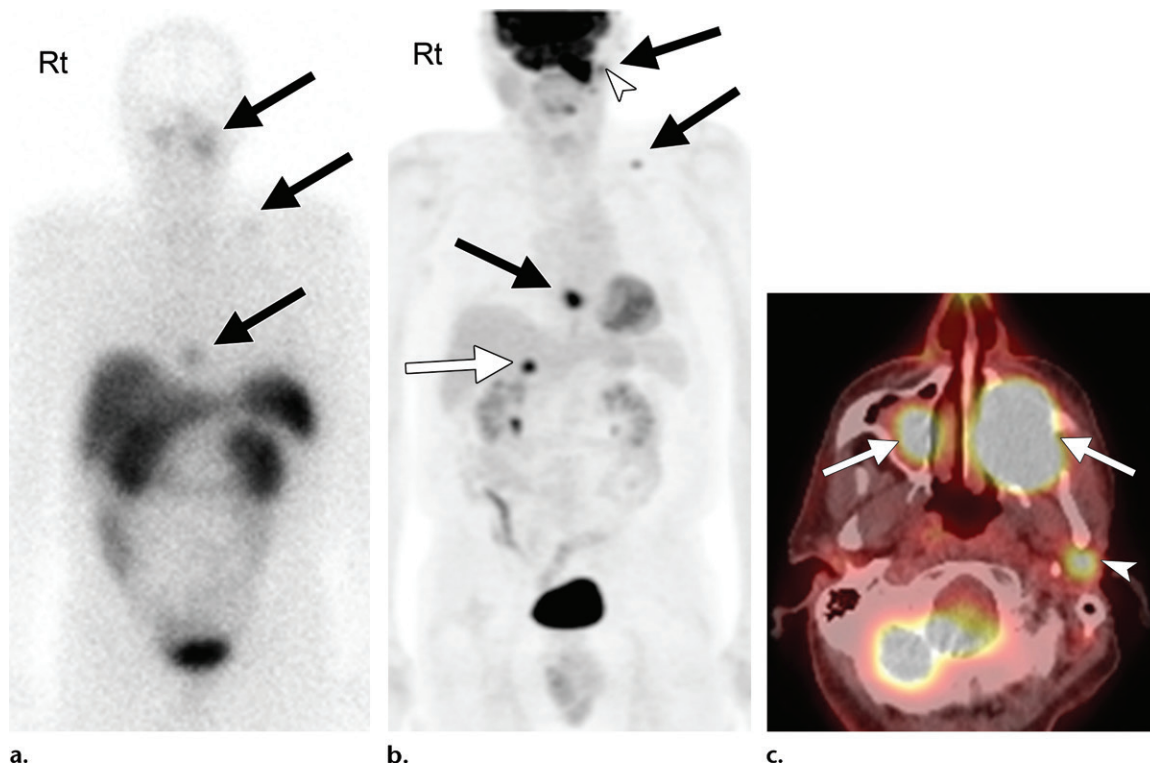


**Figure 17.**  $^{111}\text{In}$ -pentetreotide scintigraphy and  $^{18}\text{F}$ -FDG PET/CT in a 73-year-old man with MCC metastases at different sites. *Rt* = right. (a) Whole-body image from  $^{111}\text{In}$ -pentetreotide scintigraphy shows increased radiotracer uptake in the bilateral maxillary sinuses, left supraclavicular lymph node, and heart (arrows), indicating SSTR expression in these known metastasis sites. (b) Maximum intensity projection (MIP) image from  $^{18}\text{F}$ -FDG PET/CT better shows the increased radiotracer uptake in the same areas (black arrows). In addition, there is uptake in a left cervical lymph node (arrowhead) and the right adrenal gland (white arrow). (c) Axial  $^{18}\text{F}$ -FDG PET/CT image shows the hypermetabolic bilateral maxillary sinus metastases (arrows) and left cervical lymph node metastasis (arrowhead).

PET/CT (65). Physiologic radiotracer activity in the liver, spleen, or kidneys may interfere with evaluation of these sites.

Decreased sensitivity for lung lesions is likely due to the smaller size of lung lesions, which are below the resolution of PET. Evaluation of SSTR expression is important to validate targeted molecular therapy such as somatostatin analog or peptide receptor radionuclide therapy (PRRT).

### $^{18}\text{F}$ -FDG PET versus

#### $^{68}\text{Ga}$ -Somatostatin Analog PET

Currently,  $^{18}\text{F}$ -FDG is the only PET tracer indicated for imaging of MCC in the NCCN guidelines. There is no consensus on use of  $^{68}\text{Ga}$ -somatostatin analog PET for imaging of MCC. In gastrointestinal NET, there is an inverse relationship between the World Health Organization (WHO) tumor grade and the European Neuroendocrine Tumor Society (ENETS) tumor grade based on Ki-67 and SSTR expression rate (66). Ki-67 is a marker of cellular proliferation: well-differentiated tumors have lower Ki-67 level (<3%), whereas poorly differentiated tumors have higher Ki-67 level (>20%) (67). In non-MCC NETs,  $^{68}\text{Ga}$ -somatostatin analog PET/CT

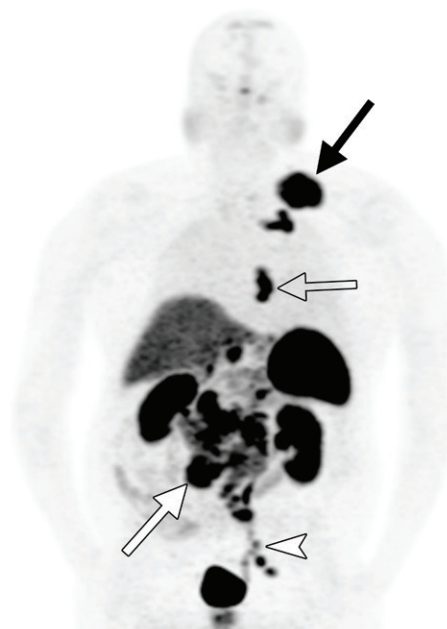
is recommended for imaging lower-grade tumors with lower Ki-67 expression and  $^{18}\text{F}$ -FDG PET is recommended for imaging higher-grade more aggressive tumors (68).

Little is known regarding an association between SSTR expression, tumor grade, and Ki-67 level in MCC. A preliminary study showed that  $^{68}\text{Ga}$ -somatostatin analog PET/CT provides good diagnostic performance equivalent to that of  $^{18}\text{F}$ -FDG PET/CT (69). These results do not suggest that  $^{18}\text{F}$ -FDG PET/CT should be replaced by  $^{68}\text{Ga}$ -SSTR imaging. However, it could be considered in select cases of SSTR-positive MCC—that is, “personalized medicine.” Further studies are needed to establish the usefulness of  $^{68}\text{Ga}$ -somatostatin analog PET for imaging of MCC.

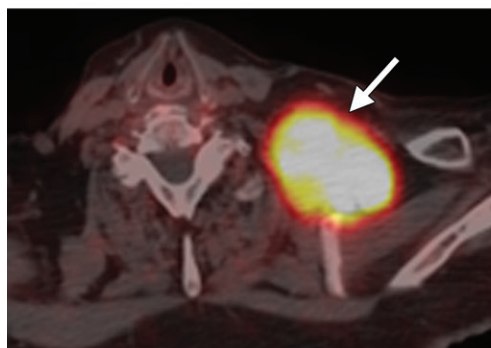
### Peptide Receptor Radionuclide Therapy

The SSTR binding peptide is paired with a  $\beta$  particle-emitting radioisotope such as yttrium 90 ( $^{90}\text{Y}$ ) or lutetium 177 ( $^{177}\text{Lu}$ ) using a chelator (bonding agent). The radiolabeled peptides are delivered directly to tumor cells via SSTR and irradiate tumor cells. In Europe, PRRT has been

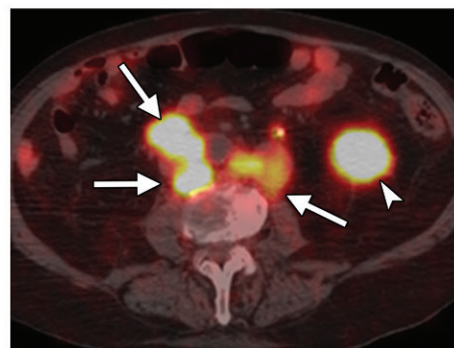
**Figure 18.** Widespread metastases with increased SSTR expression in a 70-year-old man who underwent resection of a primary MCC in the left knee. (a) Maximum intensity projection (MIP) image from  $^{68}\text{Ga}$ -DOTATATE PET shows intense radiotracer uptake in the left supraclavicular (black solid arrow), mediastinal (open arrow), retroperitoneal (white solid arrow), and left inguinal (arrowhead) stations, compatible with metastasis. (b) Axial PET/CT image shows the radiotracer-avid enlarged left supraclavicular node (arrow). (c) Axial PET/CT image shows radiotracer-avid enlarged paraaortic (arrows) and mesenteric (arrowhead) nodes.



a.



b.



c.

used for treatment of SSTR-positive metastatic well-differentiated gastrointestinal NETs since the 1990s.

Retrospective analysis has shown promising results for treatment of gastrointestinal NETs. In the United States, the FDA approved  $^{177}\text{Lu}$ -DOTATATE for treatment of gastrointestinal NETs in January 2018. Currently, there are only a few case reports that have demonstrated favorable results in MCC (70–72). A larger trial is needed to further understand the efficacy of PRRT in treatment of MCC.

### Conclusion

MCC is an aggressive skin cancer with unique characteristics both clinically and radiologically. MCPyV is causally linked to its development, and antibodies to the virus can be used as a “tumor marker” in seropositive patients. Immunotherapy is now the recommended first-line systemic therapy, but caution is needed to interpret the treatment response. MCC has neuroendocrine features with SSTR expression, which can

be used for SSTR-seeking molecular imaging and potentially theranostics (PRRT). Although MCC is rare, its incidence is steadily increasing, and radiologists should be aware of its characteristics.

**Disclosures of Conflicts of Interest.**—G.A. *Activities related to the present article:* grant from Nihon Medi-Physics. *Activities not related to the present article:* disclosed no relevant relationships. *Other activities:* disclosed no relevant relationships. P.N. *Activities related to the present article:* disclosed no relevant relationships. *Activities not related to the present article:* advisor for Merck Sharp & Dohme and EMD Serono/Pfizer; grants from EMD Serono. *Other activities:* patent pending for T-cell receptors targeting Merkel cell polyomavirus.

### References

1. Harms PW. Update on Merkel cell carcinoma. *Clin Lab Med* 2017;37(3):485–501.
2. Tang CK, Toker C. Trabecular carcinoma of the skin: an ultrastructural study. *Cancer* 1978;42(5):2311–2321.
3. Harms PW, Harms KL, Moore PS, et al. The biology and treatment of Merkel cell carcinoma: current understanding and research priorities. *Nat Rev Clin Oncol* 2018;15(12):763–776.
4. Paulson KG, Park SY, Vandeven NA, et al. Merkel cell carcinoma: current US incidence and projected increases based on changing demographics. *J Am Acad Dermatol* 2018;78(3):457–463.e2.

5. Becker JC. Merkel cell carcinoma. *Ann Oncol* 2010;21(suppl 7):vii81–vii85.
6. SEER Cancer Stat Facts. Melanoma of the skin. <https://seer.cancer.gov/statfacts/html/melan.html>. Accessed March 15, 2019.
7. Becker JC, Stang A, DeCaprio JA, et al. Merkel cell carcinoma. *Nat Rev Dis Primers* 2017;3(1):17077.
8. Paulson KG, Bhatia S. Advances in immunotherapy for metastatic Merkel cell carcinoma: a clinician's guide. *J Natl Compr Canc Netw* 2018;16(6):782–790.
9. Harms KL, Healy MA, Nghiem P, et al. Analysis of Prognostic Factors from 9387 Merkel Cell Carcinoma Cases Forms the Basis for the New 8th Edition AJCC Staging System. *Ann Surg Oncol* 2016;23(11):3564–3571.
10. Fields RC, Busam KJ, Chou JF, et al. Five hundred patients with Merkel cell carcinoma evaluated at a single institution. *Ann Surg* 2011;254(3):465–473; discussion 473–475.
11. Albores-Saavedra J, Batich K, Chable-Montero F, Sagy N, Schwartz AM, Henson DE. Merkel cell carcinoma demographics, morphology, and survival based on 3870 cases: a population based study. *J Cutan Pathol* 2010;37(1):20–27.
12. Feng H, Shuda M, Chang Y, Moore PS. Clonal integration of a polyomavirus in human Merkel cell carcinoma. *Science* 2008;319(5866):1096–1100.
13. Heath M, Jaimes N, Lemos B, et al. Clinical characteristics of Merkel cell carcinoma at diagnosis in 195 patients: the AEIOU features. *J Am Acad Dermatol* 2008;58(3):375–381.
14. Engels EA, Frisch M, Goedert JJ, Biggar RJ, Miller RW. Merkel cell carcinoma and HIV infection. *Lancet* 2002;359(9305):497–498.
15. Penn I, First MR. Merkel's cell carcinoma in organ recipients: report of 41 cases. *Transplantation* 1999;68(11):1717–1721.
16. Paulson KG, Lewis CW, Redman MW, et al. Viral oncoprotein antibodies as a marker for recurrence of Merkel cell carcinoma: a prospective validation study. *Cancer* 2017;123(8):1464–1474.
17. NCCN clinical practice guidelines in oncology: Merkel cell carcinoma (version 2.2019). National Comprehensive Cancer Network. [https://www.nccn.org/professionals/physician\\_gls/pdf/mcc.pdf](https://www.nccn.org/professionals/physician_gls/pdf/mcc.pdf). Accessed April 2, 2019.
18. Moshiri AS, Nghiem P. Milestones in the staging, classification, and biology of Merkel cell carcinoma. *J Natl Compr Canc Netw* 2014;12(9):1255–1262.
19. Nguyen BD, McCullough AE. Imaging of Merkel cell carcinoma. *RadioGraphics* 2002;22(2):367–376.
20. Lewis KG, Weinstock MA, Weaver AL, Otley CC. Adjuvant local irradiation for Merkel cell carcinoma. *Arch Dermatol* 2006;142(6):693–700.
21. Eftekhari F, Wallace S, Silva EG, Lenzi R. Merkel cell carcinoma of the skin: imaging and clinical features in 93 cases. *Br J Radiol* 1996;69(819):226–233.
22. Anderson SE, Beer KT, Banic A, et al. MRI of Merkel cell carcinoma: histologic correlation and review of the literature. *AJR Am J Roentgenol* 2005;185(6):1441–1448.
23. Peloschek P, Novotny C, Mueller-Mang C, et al. Diagnostic imaging in Merkel cell carcinoma: lessons to learn from 16 cases with correlation of sonography, CT, MRI and PET. *Eur J Radiol* 2010;73(2):317–323.
24. Dunlop P, Sapp H, Logan PM, Walsh NMG. Merkel cell carcinoma of the abdominal wall. *Skeletal Radiol* 1998;27(7):396–399.
25. Moayed S, Maldjian C, Adam R, Bonakdarpour A. Magnetic resonance imaging appearance of metastatic Merkel cell carcinoma to the sacrum and epidural space. *Magn Reson Imaging* 2000;18(8):1039–1042.
26. Hawryluk EB, O'Regan KN, Sheehy N, et al. Positron emission tomography/computed tomography imaging in Merkel cell carcinoma: a study of 270 scans in 97 patients at the Dana-Farber/Brigham and Women's Cancer Center. *J Am Acad Dermatol* 2013;68(4):592–599.
27. Concannon R, Larcos GS, Veness M. The impact of (18)F-FDG PET-CT scanning for staging and management of Merkel cell carcinoma: results from Westmead Hospital, Sydney, Australia. *J Am Acad Dermatol* 2010;62(1):76–84.
28. Bichakjian CK, Olencki T, Aasi SZ, et al. Merkel Cell Carcinoma, Version 1.2018, NCCN Clinical Practice Guidelines in Oncology. *J Natl Compr Canc Netw* 2018;16(6):742–774.
29. Sims JR, Grotz TE, Pockaj BA, et al. Sentinel lymph node biopsy in Merkel cell carcinoma: the Mayo Clinic experience of 150 patients. *Surg Oncol* 2018;27(1):11–17.
30. Liu J, Larcos G, Howle J, Veness M. Lack of clinical impact of <sup>18</sup>F-fluorodeoxyglucose positron emission tomography with simultaneous computed tomography for stage I and II Merkel cell carcinoma with concurrent sentinel lymph node biopsy staging: a single institutional experience from Westmead Hospital, Sydney. *Australas J Dermatol* 2017;58(2):99–105.
31. Kouzmina M, Koljonen V, Leikola J, Böhling T, Lantto E. Frequency and locations of systemic metastases in Merkel cell carcinoma by imaging. *Acta Radiol Open* 2017;6(3):2058460117700449.
32. Ben-Haim S, Garkaby J, Primashvili N, et al. Metabolic assessment of Merkel cell carcinoma: the role of 18F-FDG PET/CT. *Nucl Med Commun* 2016;37(8):865–873.
33. Medina-Franco H, Urist MM, Fiveash J, Heslin MJ, Bland KI, Beenken SW. Multimodality treatment of Merkel cell carcinoma: case series and literature review of 1024 cases. *Ann Surg Oncol* 2001;8(3):204–208.
34. Shoda K, Ikoma H, Yamamoto Y, et al. A case of long-term survival following hepatectomy for liver metastasis of Merkel cell carcinoma. *Surg Case Rep* 2015;1(1):30.
35. Tirumani SH, Shinagare AB, Sakellis C, et al. Merkel cell carcinoma: a primer for the radiologist. *AJR Am J Roentgenol* 2013;200(6):1186–1196.
36. Nguyen BD, McCullough AE. Isolated Tibial Metastasis from Merkel Cell Carcinoma. *Radiol Case Rep* 2015;2(4):88.
37. Maugeri R, Giugno A, Giammalva RG, et al. A thoracic vertebral localization of a metastasized cutaneous Merkel cell carcinoma: case report and review of literature. *Surg Neurol Int* 2017;8(1):190.
38. Kitajima K, Nakamoto Y, Okizuka H, et al. Accuracy of whole-body FDG-PET/CT for detecting brain metastases from non-central nervous system tumors. *Ann Nucl Med* 2008;22(7):595–602.
39. Honeybul S. Cerebral metastases from Merkel cell carcinoma: long-term survival. *J Surg Case Rep* 2016;2016(10).
40. Abul-Kasim K, Söderström K, Hallsten L. Extensive central nervous system involvement in Merkel cell carcinoma: a case report and review of the literature. *J Med Case Reports* 2011;5:35.
41. Barkdull GC, Healy JF, Weisman RA. Intracranial spread of Merkel cell carcinoma through intact skull. *Ann Otol Rhinol Laryngol* 2004;113(9):683–687.
42. Ng G, Lenehan B, Street J. Metastatic Merkel cell carcinoma of the spine. *J Clin Neurosci* 2010;17(8):1069–1071.
43. Palestro CJ. FDG-PET in musculoskeletal infections. *Semin Nucl Med* 2013;43(5):367–376.
44. Vijay K, Venkateswaran K, Shetty AP, Rajasekaran S. Spinal extra-dural metastasis from Merkel cell carcinoma: a rare cause of paraplegia. *Eur Spine J* 2008;17(suppl 2):S267–S270.
45. Turgut M, Gökpınar D, Barutça S, Erkus M. Lumbosacral metastatic extradural Merkel cell carcinoma causing nerve root compression: case report. *Neurol Med Chir (Tokyo)* 2002;42(2):78–80.
46. Tello TL, Cogshall K, Yom SS, Yu SS. Merkel cell carcinoma: an update and review—current and future therapy. *J Am Acad Dermatol* 2018;78(3):445–454.
47. Iyer JG, Blom A, Doumani R, et al. Response rates and durability of chemotherapy among 62 patients with metastatic Merkel cell carcinoma. *Cancer Med* 2016;5(9):2294–2301.
48. Nghiem PT, Bhatia S, Lipson EJ, et al. PD-1 Blockade with Pembrolizumab in Advanced Merkel-Cell Carcinoma. *N Engl J Med* 2016;374(26):2542–2552.
49. Hodi FS, Ballinger M, Lyons B, et al. Immune-Modified Response Evaluation Criteria In Solid Tumors (imRECIST): Refining Guidelines to Assess the Clinical Benefit of Cancer Immunotherapy. *J Clin Oncol* 2018;36(9):850–858.
50. Broski SM, Young JR, Kendi AT, Subramaniam RM. Skeletal Metastasis Evaluation: Value and Impact of PET/Computed Tomography on Diagnosis, Management and Prognosis. *PET Clin* 2019;14(1):103–120.
51. Treglia G, Kakhki VR, Giovannella L, Sadeghi R. Diagnostic performance of fluorine-18-fluorodeoxyglucose positron

- emission tomography in patients with Merkel cell carcinoma: a systematic review and meta-analysis. *Am J Clin Dermatol* 2013;14(6):437–447.
52. Nakamoto Y, Cohade C, Tatsumi M, Hammoud D, Wahl RL. CT appearance of bone metastases detected with FDG PET as part of the same PET/CT examination. *Radiology* 2005;237(2):627–634.
  53. Siva S, Byrne K, Seel M, et al. 18F-FDG PET provides high-impact and powerful prognostic stratification in the staging of Merkel cell carcinoma: a 15-year institutional experience. *J Nucl Med* 2013;54(8):1223–1229.
  54. Poulsen M, Macfarlane D, Veness M, et al. Prospective analysis of the utility of 18-FDG PET in Merkel cell carcinoma of the skin: a Trans Tasman Radiation Oncology Group study, TROG 09:03. *J Med Imaging Radiat Oncol* 2018;62(3):412–419.
  55. George A, Girault S, Testard A, et al. The impact of (18) F-FDG-PET/CT on Merkel cell carcinoma management: a retrospective study of 66 scans from a single institution. *Nucl Med Commun* 2014;35(3):282–290.
  56. Byrne K, Siva S, Chait L, et al. 15-Year Experience of 18F-FDG PET Imaging in Response Assessment and Restaging After Definitive Treatment of Merkel Cell Carcinoma. *J Nucl Med* 2015;56(9):1328–1333.
  57. Eshghi N, Lundeen TF, MacKinnon L, Avery R, Kuo PH. 18F-FDG PET/CT for Monitoring Response of Merkel Cell Carcinoma to the Novel Programmed Cell Death Ligand 1 Inhibitor Avelumab. *Clin Nucl Med* 2018;43(5):e142–e144.
  58. Vellani C, D'Ambrosio D, Licata L, Vacchieri I, Bernardo A, Trifirò G. Monitoring response of advanced Merkel cell carcinoma to avelumab with <sup>18</sup>F-FDG PET/CT. *Eur J Nucl Med Mol Imaging* 2019;46(5):1197–1198.
  59. Ziessman H, O'Malley J, Thrall JH, Fahey F. *The requisites: nuclear medicine*. 4th ed. Philadelphia, Pa: Elsevier, 2014.
  60. Rosenthal DI. Radiologic diagnosis of bone metastases. *Cancer* 1997;80(8 suppl):1595–1607.
  61. Rong J, Wang S, Ding Q, Yun M, Zheng Z, Ye S. Comparison of 18 FDG PET-CT and bone scintigraphy for detection of bone metastases in breast cancer patients: a meta-analysis. *Surg Oncol* 2013;22(2):86–91.
  62. Qu X, Huang X, Yan W, Wu L, Dai K. A meta-analysis of <sup>18</sup>F-FDG-PET-CT, <sup>18</sup>F-FDG-PET, MRI and bone scintigraphy for diagnosis of bone metastases in patients with lung cancer. *Eur J Radiol* 2012;81(5):1007–1015.
  63. Xu C, Zhang R, Zhang H, Zhang Z. Comparison of <sup>18</sup>F-FDG PET/PET-CT and bone scintigraphy for detecting bone metastases in patients with nasopharyngeal cancer: a meta-analysis. *Oncotarget* 2017;8(35):59740–59747.
  64. Gardair C, Samimi M, Touzé A, et al. Somatostatin Receptors 2A and 5 Are Expressed in Merkel Cell Carcinoma with No Association with Disease Severity. *Neuroendocrinology* 2015;101(3):223–235.
  65. Buder K, Lapa C, Kreissl MC, et al. Somatostatin receptor expression in Merkel cell carcinoma as target for molecular imaging. *BMC Cancer* 2014;14(1):268.
  66. Hofman MS, Lau WFE, Hicks RJ. Somatostatin receptor imaging with <sup>68</sup>Ga DOTATATE PET/CT: clinical utility, normal patterns, pearls, and pitfalls in interpretation. *Radiographics* 2015;35(2):500–516.
  67. Klimstra DS, Modlin IR, Coppola D, Lloyd RV, Suster S. The pathologic classification of neuroendocrine tumors: a review of nomenclature, grading, and staging systems. *Pancreas* 2010;39(6):707–712.
  68. Hope TA, Bergsland EK, Bozkurt MF, et al. Appropriate Use Criteria for Somatostatin Receptor PET Imaging in Neuroendocrine Tumors. *J Nucl Med* 2018;59(1):66–74.
  69. Taralli S, Sollini M, Milella M, et al. <sup>18</sup>F-FDG and <sup>68</sup>Ga-somatostatin analogs PET/CT in patients with Merkel cell carcinoma: a comparison study. *EJNMMI Res* 2018;8(1):64.
  70. Basu S, Ranade R. Favorable Response of Metastatic Merkel Cell Carcinoma to Targeted <sup>177</sup>Lu-DOTATATE Therapy: Will PRRT Evolve to Become an Important Approach in Receptor-Positive Cases? *J Nucl Med Technol* 2016;44(2):85–87.
  71. Salavati A, Prasad V, Schneider CP, Herbst R, Baum RP. Peptide receptor radionuclide therapy of Merkel cell carcinoma using (<sup>177</sup>)lutetium-labeled somatostatin analogs in combination with radiosensitizing chemotherapy: a potential novel treatment based on molecular pathology. *Ann Nucl Med* 2012;26(4):365–369.
  72. Meier G, Waldherr C, Herrmann R, Maecke H, Mueller-Brand J, Pless M. Successful targeted radiotherapy with <sup>90</sup>Y-DOTATOC in a patient with Merkel cell carcinoma: a case report. *Oncology* 2004;66(2):160–163.